A Study on the Design of LOx Turbopump Inducers

Lucrezia Veggi, Julian D Pauw, Bernd Wagner, Oskar Haidn

A Study on the Design of LOx Turbopump Inducers

Lucrezia Veggi[1]*, Julian D. Pauw[1], Bernd Wagner[2], Oskar J. Haidn[1]

ISROMAC 2017

International Symposium on Transport Phenomena and Dynamics of Rotating Machinery

Maui, Hawaii

December 16-21, 2017

Abstract

In this paper, the design methodology for turbopump components is presented and the design process of the inducer for a LOX turbopump is discussed in detail. The design methodology is based on classical methods and results of more recent studies. With the design process presented here, three inducers have been designed and numerically investigated. The aim of the study is to analyze the influence of the incidence angle on the performance by linking cavitation behavior and internal flow phenomena of the inducer. Results show that with increasing incidence angle, the cavitation formation increases causing flow deflection in the blade passage. These flow phenomena provoke flow separation on the blade pressure side and increase the tendency of the flow to separate near the hub at the trailing edge.

Keywords

Inducer — Design — Cavitation — Internal flow — CFD

[1] *Department of Mechanical Engineering, Chair of Turbomachinery and Flight Propulsion, Division of Space Propulsion, Technical University of Munich, Munich, Germany*

[2] *DLR-Institute of Space Propulsion, Lampoldshausen, Germany*

*__Corresponding author__: lucrezia.veggi@ltf.mw.tum.de

INTRODUCTION

The need of high thrust levels for future space transportation systems results in high combustion chamber pressures in liquid rocket engines. The advantage of pump-fed over pressure-fed engines consists in the requirement of relatively low pump inlet pressures, and thus propellant tank pressures. The major part of the pressure required in the chamber is supplied by the pumps. The use of turbopumps results in a decrease of system weight and an increase of performance as compared to pressurized-gas fed systems. Both dimensions and performance of the turbopump depend on the engine cycle and the requirements of the combustion chamber. Due to the high rotational speeds in the pump, the fluid pressure might drop below the vapor pressure resulting in cavitation. This flow phenomenon can lead to unstable operating conditions and pump failure. Rocket propellant fed turbopumps have inducers in order to avoid cavitation, improve the suction performance and reduce the propellant tank pressure and weight. The main task of the inducer is to provide a modest increase in pressure upstream of the main pump, typically a radial impeller, which in turns prevents cavitation and allows sufficiently reasonable operating conditions in the main pump.

First documents describing the design of inducers for liquid rocket engines came from the United States in the 1960s-70s [1, 2] where recommended ranges of relevant geometric parameters were given. Based on studies that have followed in the years, Acosta [3] summarized in the early 1990s results concerning inducer design, performance, flow phenomena as well as system stability. In the last two decades, numerous experimental and numerical studies have been conducted on the impact of geometric variations on the performance. Acosta [4], Bakir [5] and Cervone [6] made some efforts to understand the influence of the leading edge sweep on the performance in cavitating regimes, whereas Coutier-Delgosha [7] published results on the impact of the leading edge shape on the cavitation behavior. The effect of tip clearance on inducer performance has been investigated e.g. by Hong [8] and Kim [9]. The common characteristic of these studies is the focus on the effect of geometric variations on cavitation behavior and performance. However, a detailed analysis of the flow phenomena inside the blade passage, which is influenced by cavitation and has an impact on the inflow of the main pump, is rarely covered in the literature. A detailed study of flow phenomena inside rocket pump inducers has been conducted by Lakshminarayana [10], however operating the inducer with air in non-cavitating regime in the experimental setup.

Within the frame of the research project KonRAT at the Technical University of Munich (TUM), where a LOX turbopump for a LH_2/ LOX expander cycle engine is investigated [11], a design methodology for turbopump components has been developed. The design process for the pump and especially the design of inducers are discussed in detail. The design methodology is based on classical methods derived from the NASA documents [1, 2], however taking into account more recent studies for the choice of some design parameters.

The intention of the authors is to initiate a process for a better comprehension of the link between the cavitation behavior and the complex fluid mechanics inside the blade passage. The approach applied to achieve this goal is to re-

duce the inducer geometry to its simplest form in order to limit the parameters responsible for flow phenomena, isolate individual effects and dissolve their dependencies. The study presented in this paper is the first step taken towards this direction. Three flat-plate inducers have been designed with a variation of the blade angle at the inlet and have been numerically investigated. During the analysis particular attention has been paid to the influence of the incidence angle on the fluid mechanics inside the blade passage along with the occurence of blade cavitation.

1. INDUCER DESIGN METHODOLOGY

1.1 Pump Specification

The inducers investigated in the frame of this study are designed to meet the requirements of a LOX turbopump for a LOX/LH2 expander cycle engine with a thrust in the order of magnitude of the VINCI upper stage engine. The operational parameters of the turbopump at the design point were extrapolated from other works, e.g. [12, 13, 14], dealing with cryogenic expander cycle engines in the thrust class of VINCI. The operational conditions on the pump side at design point are listed in Table 1.

Table 1. LOX pump operating conditions

Pump requirements		
Rotational speed	20,000	rpm
Nominal mass flow rate	25	kg/s
Temperature at pump inlet	90	K
Total pressure at pump inlet	2.5	bar
Total pressure at pump outlet	~70	bar

Depending on the engine requirements listed above, the specific speed (Eq. 1) can be calculated and the pump efficiency estimated by means of empirical correlations taken from Gülich [15]. On the base of the $N_s - D_s$–diagram, the specific diameter is obtained giving a first guess of the outer pump diameter. Additionally, the shaft diameter and the impeller hub diameter at inlet are derived from similar published pump designs and kept fixed. According to Huzel [16], if the suction specific speed at inlet exceeds 10,000 or 200 in SI-units, an inducer is needed in order to improve the suction performance. Similar values are given also by Lakshminarayana [17] decreasing the limit to 8,000 or 155 in SI-units. Evaluating the suction specific speed of the pump based on Jakobsen [2], see Equation 2, indeed confirms the need of an inducer for this particular pump. Having a first estimation of the main geometrical dimensions and the configuration of the pump, a more detailed design follows. Table 2 summarizes the pump characteristics necessary for the design process.

$$N_s = N \cdot \frac{\sqrt{Q}}{H^{3/4}} \tag{1}$$

$$N_{ss} = N \cdot \frac{\sqrt{Q}}{NPSH^{3/4}} \tag{2}$$

Table 2. Pump design parameters

Quantity	Parameter	Value
Specific speed (SI)	$N_s(-)$	26.34
Pump overall efficiency	η_P (-)	0.75
Hydraulic efficiency	η_{hyd} (-)	0.88
Specific diameter (SI)	D_s (-)	0.112
Suction specific speed (SI)	N_{ss} (-)	421.2
Design head coefficient	ψ_P (-)	0.61
Design flow coefficient	ϕ_P (-)	0.0987

1.2 Design Process

The preliminary design of the inducer is part of an iterative design process involving all relevant components of the pump such as inducer, impeller, diffuser and volute. The preliminary design of the pump matches the requirements and characteristics presented in Table 1 and 2 and starts with the sizing of the impeller by assuming some parameters that are iteratively adjusted.

In the first loop of the pump design, a swirl free flow upstream of the impeller is assumed considering a pump configuration without inducer. Once the main geometrical dimensions of the impeller are calculated, these are used as input for the design of the inducer and the diffuser. From the second loop in the design process, once the inducer dimensions are known, velocities and flow angles at inducer exit can be calculated. Simplifyingly assuming that in the axial clearance distance between inducer and impeller the flow does not redistribute, the velocities and the flow angles at inducer outlet are used to correct the previous assumption of a swirl free flow upstream of the impeller. Figure 1 shows schematically the design process.

The sizing of the inducer is strictly dependent on the geometrical dimensions resulting from the preliminary design of the impeller. Depending on the head rise of the inducer, one differentiates between low head ($\psi \leq 0.15$) and high head ($\psi > 0.15$) inducers. In the presented design methodology the head rise capability of the inducer is an assumption made at the very beginning of the inducer design. Sutton provides a guideline value for the pressure increase in the inducer of typically 10% of the total pump pressure rise [18]. According to Logan, simple inducers with noncambered blading, so called flat-plate inducers, where the blade exit angle is equal to the blade inlet angle, have head coefficients limited to values around 0.08 [19]. When the geometry becomes more complex by introducing e.g. cambered blading or a tapered hub contour, the head rise capability of the inducer increases.

Since the goal of this study is to better understand the influence of single design parameters on the internal flow

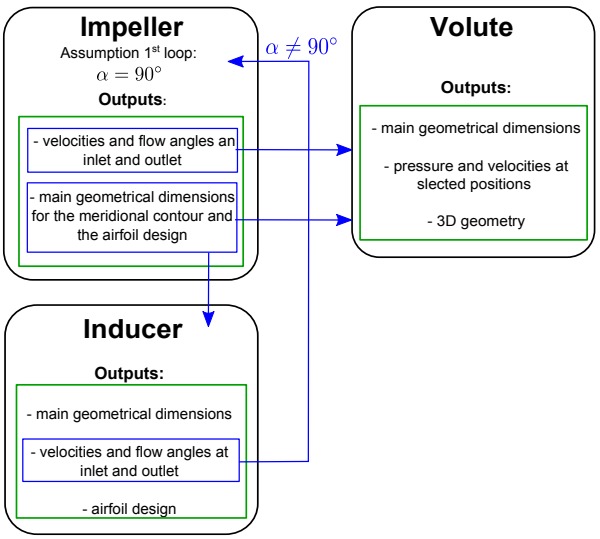

Figure 1. Design process of the pump components

and therefore on the performance of the inducer, the first design of the inducer has to be as simple as possible with complexity being introduced step by step. Consequently, the geometries used for this study are flat-plate inducers with cylindrical hub and tip, which means that the hub and tip diameters are constant from inlet to outlet. The head rise capability of the inducer must be sufficient to deliver the demanded 10% of the total pump pressure rise.

These assumptions for the pump requirements, shown in Table 2, result in a head coefficient of 0.107. For low-head inducers the inducer discharge dimensions must match those of the impeller eye [2]. The hub-to-tip diameter ratio at the inducer outlet is estimated by means of the $d_{t1}/d_{t2} - N_s$–diagram given in the NASA document SP-8052 [2]. The tip diameter is derived at the impeller inlet and at inducer outlet with the hub diameter kept fixed

The sizing of the inducer blade profiles is based on the assumption that the flow can be described by potential flow models. These models assume a two-dimensional, irrotational, steady flow of an incompressible inviscid flow through a two-dimensional blade cascade [2]. The tridimensional inducer blade is derived from the design of blade cascades at different heights between hub and shroud. Once the geometrical dimensions and characteristics of the inducer are known, the conditions of the entering and leaving flows necessary for the cascade geometry design are easily calculated by means of velocity triangles. Figure 2 shows the blade cascade geometry in a certain radial position with inlet and outlet conditions as well as characteristic flow parameters. Characteristic geometric parameters of the cascade are blade chord length C, blade spacing along the cascade axis S, blade angle β, incidence angle i and deviation angle δ. In order to obtain these parameters a number of assumptions is necessary.

First, the number of blades Z has to be fixed. Pumping high-density fluids requires:

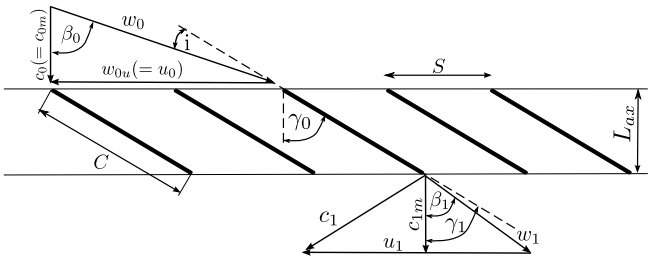

Figure 2. Blade cascade geometry and flow parameters

- Large blade chord lengths to provide adequate bending strength to withstand the high hydraulic loads. Moreover, the larger the blade chord length the higher is the residence time for the collapse of cavitation bubbles and for the gradual addition of energy before entering the impeller.

- Large blade spacing in order to obtain a small ratio of blade thickness to blade spacing to accommodate the blade thickness inside the cavity and to minimize the blockage.

These requirements are equivalent to a requirement for low blade numbers. In the literature, different recommendations can be found: the document of the NASA [2] suggests a number between two and five, Huzel [16] and Lakshminarayana [17] recommend three to four for better suction performance. For this study a two-bladed inducer has been chosen.

In the next step of the design process, the inducer blade angle has to be defined. For a flat-plate inducer, once the blade angle at inlet is derived, it is simply kept constant along the blade chord. Using a flat-plate inducer, to generate an increasing pressure rise results in increasing inlet incidence angles with the consequence of high losses and large-scale cavitation. Gülich [15] suggests inlet incidence angles between 2° and 4°. Acosta [3] and Lakshminarayana [17] just give blade angle ranges between 70° and 85° (axial definition). In the NASA document [2], the ratio of incidence angle to blade angle (circumferential definition) ν_B should lie in the range of 0.35 and 0.5. For thin blades the ratio should be 0.35 and for thick blades 0.5. The recommended design value is the mean of 0.425.

In the design process two possibilities have been implemented to fix the blade angle:

1. The ratio ν_B is assumed and kept fixed along the entire radius

2. Incidence angles at hub and tip are assumed. The incidence angle at the hub must be greater than at the tip and the gradient in between is linear.

A further assumption in the design process is related to the solidity. The solidity is the ratio of blade chord length to blade spacing. For flat-plate inducers, the solidity is supposed to stay constant over the radius. According to Gülich [15] and

Jakobsen [2], for better suction performance current practice requires solidity values between 2 and 3. With the solidity kept constant over the radius, further geometry parameters such as blade chord, blade axial length and angular wrap angle θ, can be derived. However, the parameter values calculated at this point of the process could change depending on upcoming decisions related to the inducer geometry. The solidity and therefore the blade chord and axial length can be affected by the leading edge and the trailing edge shapes. Very often, inducers present a swept back contour at the leading edge, which positively affects the suction performance and the cavitation behavior. When introducing a sweep back at the leading edge, the loss in solidity should be compensated with a corresponding increase in axial length in such way that the solidity is maintained at its full value. Similarly, the trailing edge geometry has an impact on solidity, blade chord and blade axial length.

To complete the set of geometrical parameters necessary for the tridimensional design of the blade, the blade thickness has to be defined. Both hydrodynamic and structural design considerations determine the blade thickness resulting in a tapered form with the maximum at the juncture with the hub and the minimum at the tip [2]. Gülich [15] suggests a ratio of the blade thickness at the tip to the tip diameter between 0.016 and 0.022, keeping in mind that these values are related to industrial pumps where manufacturing differs from that applied in aerospace. However, evaluating available data from the literature [5, 20, 21, 22], this ratio seems to be observed also in aerospace applications.

2. INDUCER GEOMETRIES

In this study, three flat-plate inducers with cylindrical hub and tip have been investigated. The primary goal is to investigate the influence of the blade angle on the flow and on the suction performance. In order to better recognize the influence of a variation of the blade angle on the internal flow, the geometries were designed to have as many as possible geometrical parameters in common.

The inducers do not have a sweep back at the leading edge. Nevertheless, the blade geometry does include an increase in axial length, since it is intended to introduce a sweep back at the leading edge in future studies and use the geometries presented here as a reference for the comparison of suction performance. All geometries have been designed to present the same angular wrap angle θ_{TE} at the trailing edge at any blade height. A thickness ratio of 0.015 has been applied resulting in a blade thickness at the tip of 1.1 mm. For all inducer geometries, the same value of blade chord length is applied at the tip.

The tip clearance of all three inducers has been set to a constant value of 0.25 mm which corresponds to 1.94% of the blade height. The decision was taken considering the work of Jakobsen [2] who recommends a maximal clearance area of 3% of the flow area. Here, the clearance area results in 2.44% of the flow area.

As mentioned above, the only parameter that has been actively varied is the blade angle at inlet. Nevertheless, other parameters such as blade chord, blade axial length and angular wrap angle, are functions of the blade angle. A variation of its value inevitably leads to a variation of the related parameters. Moreover, the constraint of constant angular wrap angle over the radius at the trailing edge (see previous paragraph) results in different trailing edge shapes.

For the design of the first geometry (inducer A), the blade angle has been defined by assuming a ratio ν_B of 0.425, fixed throughout the entire blade height. The blade chord length at the tip of inducer A is the reference value for the design of the other geometries. For inducer B the ratio ν_B has been decreased to 0.35, which, according to Jakobsen [2], is the minimum recommended value. In this way the incidence angles are decreased and the blade angles increased. For inducer A and B, the parameter variations result in a slightly backward swept trailing edge geometry as shown in the meridional view in Figure 3.

The incidence angles of inducer A and B are far from the recommended range of 2° ... 4°. Therefore, the geometry of inducer C has been designed with the second approach for the blade angle definition, namely by assuming an incidence angle of 4° at hub and of 3° at tip. Figure 4 shows a comparison of blade angles (left) and incidence angles (right) along the radius for the three geometries. The trailing edge geometry of inducer C is shown in Figure 3 and presents characteristics of a forward swept trailing edge.

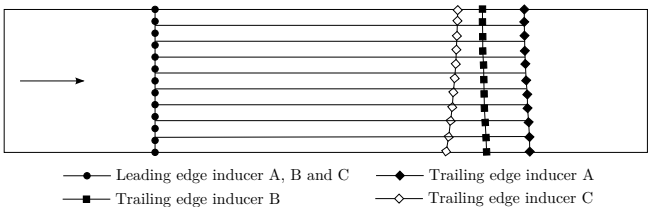

Figure 3. Comparison of the inducers geometries in the meridional view

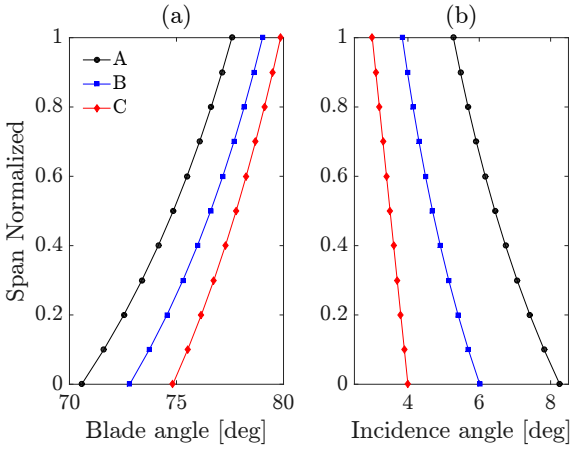

Figure 4. Comparison of: (a) blade angle and (b) incidence angle along the radius

Table 3. Main constructive parameters of the inducers

Flow coefficient [-]		0.125	
Head coefficient [-]		0.107	
Blade number [-]		2	
Hub diameter [mm]		45	
Tip diameter [mm]		70.83	
Hub-to-tip ratio [-]		0.634	
Blade chord length at tip [mm]		277	
Blade thickness at tip [mm]		1.1	
	Inducer A	Inducer B	Inducer C
Incidence-blade angle ratio ν_B [-]	0.425	0.35	-
Blade angle at tip [°]	77.6	79	79.8
Blade angle at hub [°]	70.6	72.8	74.8
Incidence at tip [°]	5.3	3.8	3
Incidence at hub [°]	8.3	6	4
Solidity at tip [-]	2.49	2.49	2.49
Solidity at hub [-]	2.58	2.56	2.54
Blade axial length at hub [mm]	60.5	53.3	47
Angular wrap angle [°]	437.7	440	441.2

It is also clear, that in a flat-plate inducer an increase of the blade angle at inlet while keeping the blade chord length at the tip constant inevitably results in a decrease of blade axial length. All inducers present an elliptic geometry at the leading edge as well as at the trailing edge. The main constructive parameters are summarized in Table 3.

3. COMPUTATIONAL METHODOLOGY

The three-dimensional incompressible flow calculation of the inducer was performed in ANSYS®CFX 16.2. For all computations a block structured mesh of around 350,000 elements has been used. The mesh was created with the mesh generator ANSYS®TurboGrid. Figure 5 shows the applied computational mesh.

For all numerical simulations, the tip clearance was not implemented. Although being aware of the impact of tip clearances on the pump performance, the neglection of the tip clearance was motivated by the intention to suppress the tip vortex due to the following reasons. The tip vortex interacts with the main flow and this interaction would have interfered with the detection of small changes in the flow due to blade angle variations. Furthermore, tip clearance leads to tip clearance and tip vortex cavitation in the peripheral zone, e.g. at the casing. The presented inducers have a radial leading edge design with the consequence that the blade cavitation is limited to the periphery of the inducer [23]. The superposition of blade cavitation and tip vortex cavitation makes the detection of changes of the blade cavitation due to blade angle variation very difficult.

The geometrical domain has been modeled as a rotating fluid domain. The casing is specifed as a counter-rotating wall so that the wall boundary is assumed to be stationary with respect to the stationary frame and in relative rotation against the fluid.

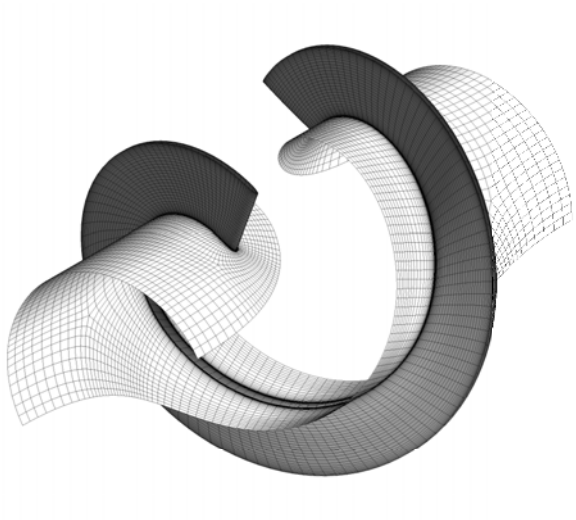

Figure 5. Computational grid of inducer A

The inducers have been simulated in steady state at the design point. Since alternate blade cavitation is not expected, one single passage has been calculated using rotational periodicity for the connection between the periodic boundaries. This approach is widely used for CFD in turbomachinery and has shown good agreement with experimental results in prediciting the correct trends of performance and the size and location of blade cavitation [24, 25].

The inlet was positioned 25 mm upstream of the leading edge and the outlet 80 mm downstream of the leading edge. At the inducer inlet, total pressure and total temperature were set. The total pressure was set to a constant value of 2.5 bar. At the inducer outlet the mass flow rate was used

as boundary condition with a value of 25 kg/s. All simulations were made with a fluid model of liquid oxygen at 90 K. The standard SST model was used for modelling turbulence. For all the numerical simulations cavitation has been taken into account by using the cavitation model implemented in ANSYS®CFX, which is a multiphase model based on the use of the Rayleigh-Plesset equation to estimate the rate of vapor production. In order to achieve convergence while the cavitation model is turned on, the following steps have been undertaken: First, an incompressible solution without cavitation with a total pressure at the inlet much higher than the desired one is computed. Here, the initial total pressure used was 10 bar. Then, from this non-cavitating initial solution, the cavitation model is turned on and the total pressure at the inlet is decreased by steps of 2.5 bar until the desired value is reached.

4. RESULTS AND DISCUSSION

The inducer geometries have been evaluated in terms of pressure rise capability, cavitation behavior and flow distribution in the blade passage.

Streamwise distribution of velocities and pressures

The absolute and axial velocities distributions as well as the total pressure distribution from inlet to outlet at midspan are summarized in Figure 6.

As expected, the pressure rise decreases with decreasing incidence angle, so that inducer C presents the lowest total pressure at outlet. However, comparing the resulting total pressures of the geometries with the design value, inducer C approximates the design value the most. It seems that for the design of a flat-plate inducer with the requirement of 10% of the total pump pressure rise, the recommended value for the ratio ν_B of 0.425 results in incidence angles larger than necessary. Inducer B, which has been designed with a ratio ν_B of 0.35, also shows too high pressure rise. The choice of incidence angles in the suggested range of 2° to 4° is the most suitable option here. Looking at the development of the total pressure in axial direction in Figure 6, for all the geometries the most of the pressure rise occurs within the first 1/3 of the chord length, which is consistent with the measurements of Lakshminarayana [10]. All inducers present a peak with a following decrease of total pressure. Absolute and axial velocity exhibit the same behavior, most pronounced for inducer A. This effect is related to the occurrence of cavitation on the suction side of the inducer blade.

Figure 8 shows in the blade to blade view the distribution of the vapor volume fraction near the hub, at midspan and near the tip for the three inducers. A further analysis at the same spanwise positions has shown that in the region where the vapor volume fraction is near or equal to one the static pressure drops below the vapor pressure, confirming the presence of cavitation. Firstly, it can be observed that a variation of the blade angle has a much higher impact at the hub than at the tip. Comparing the distribution of vapor volume fraction of inducer A with that of inducer C at tip, the decrease of cavitation is visible but limited, whereas at the hub the variation of blade angle of inducer C results in a blade suction side almost free of cavitation.

Secondly, Figure 8 shows that, independently from the geometry, cavitation covers the blade suction side up to the circumferential position where the adjacent blade begins. At midspan and below cavitation even extents into the blade passage. Consequently, the actual cross-sectional area at the entrance of the blade passage is reduced, increasing suddenly where the cavitation region ends. This causes a recirculation zone directly downstream of the cavitation region on the suction side and a flow deflection towards the axial direction which explains the strong increase of axial velocity and consequently of absolute velocity in Figure 6. Furthermore, the flow deflection from pressure side to suction side provokes downstream flow separation on the blade pressure side followed by reattachment of the flow. The distribution of relative velocity at midspan in Figure 9(b) visualizes the flow phenomena described above.

Spanwise distribution of velocities

Figure 7 shows a comparison of the three inducers in terms of tangential velocity (absolute), axial velocity and relative flow angle along the radius. The velocities and the flow angle are circumferentially mass flow averaged and evaluated directly downstream of the trailing edge and directly upstream of the outlet surface.

For all geometries, the axial velocity shows the biggest discrepancy in slope between numerical results and design value. In the hub region velocity shows a tendency of the flow to separate, while its maximum values develop near the tip. This observation is consistent with the experimental results of Lakshminarayana [10]. The three geometries show similar behavior, however near the hub the distribution of axial velocity of inducer C is gradual, whereas for inducer A and B the axial velocity further strongly decreases. A redistribution of the axial velocity from the trailing edge towards the outlet can be observed for all the inducers especially in the near wall regions.

According to Lakshminarayana [10], the tendency to separate near the hub is caused primarily by radial flows in the wake and secondary flows inside the blade passage. Here, a clear correlation between the radial and the axial velocities could not be found. A closer look at the distribution of axial velocity on a surface directly downstream of the trailing edge, given in Figure 10, reveals localized zones of low axial velocities. These regions are located in the middle of the blade passage in the lower half of the blade height. Figure 10 shows the axial velocity distribution for inducer A (left) and inducer C (right). For inducer A the axial velocity presents lower values over a bigger area.

The low axial velocity regions arise from the flow deflection in the second half of the blade passage. As already seen in the previous paragraph, at the entrance of the blade passage a flow from pressure side to suction side of the blade causes flow separation. In the second half of the blade passage the flow again undergoes a deflection, however from

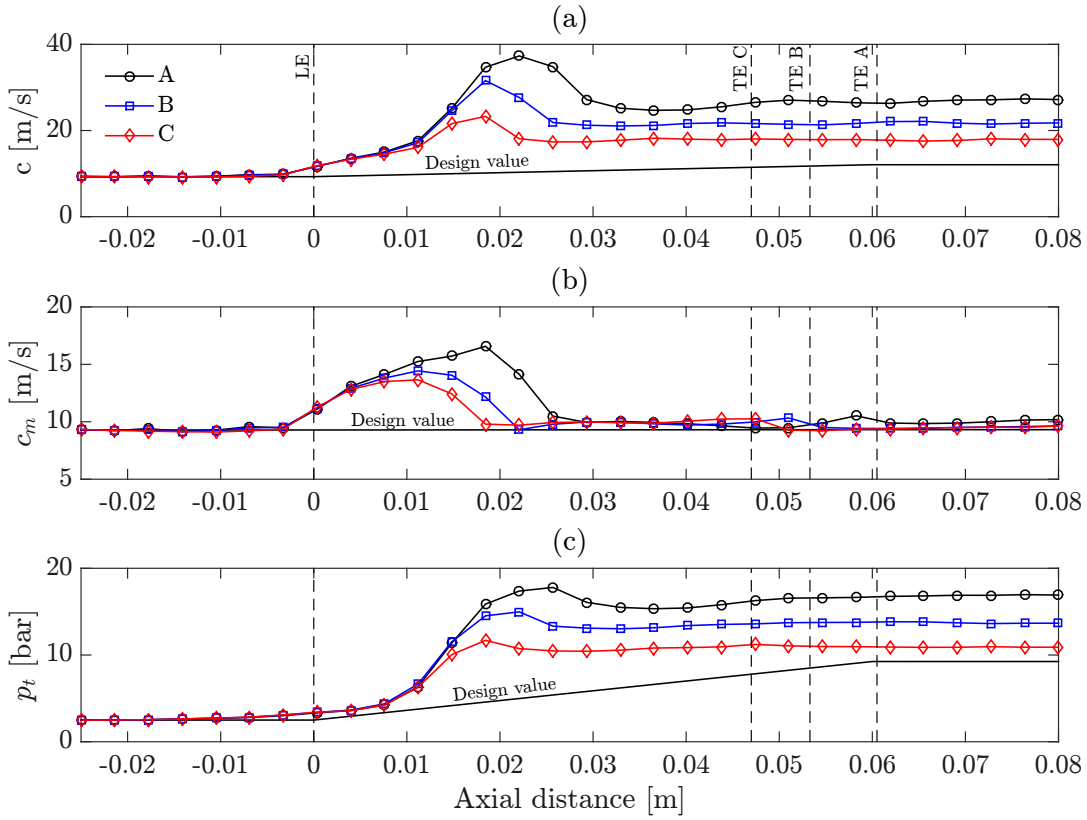

Figure 6. Velocities and total pressure distribution from inlet to outlet at midspan

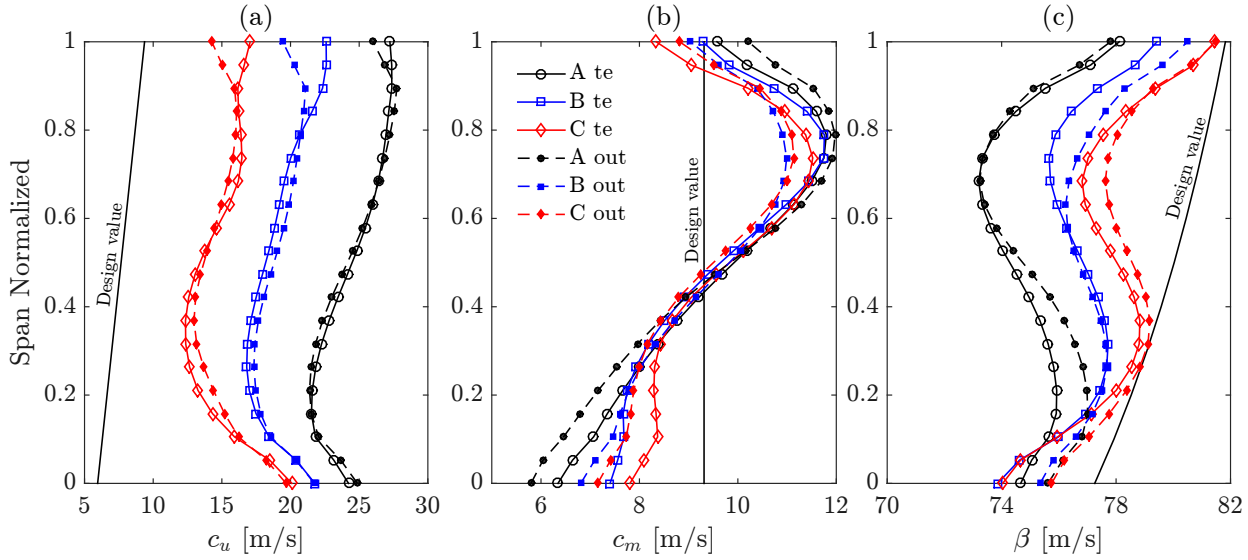

Figure 7. Velocities and flow angle distribution along the radius: (a) Tangential velocity (absolue), (b) Axial velocity and (c) Relative flow angle

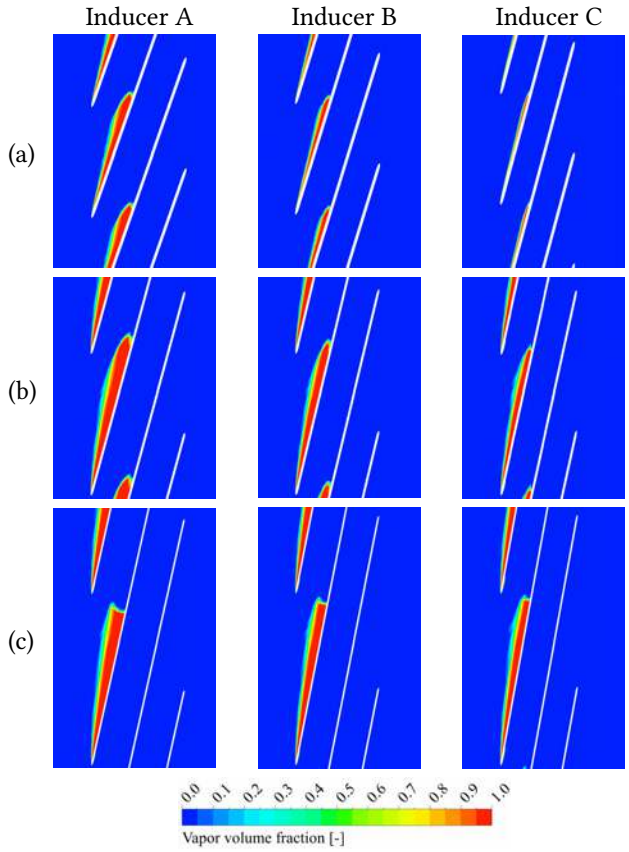

Figure 8. Vapor volume fraction contours at: (a) 2% span, (b) 50% span and (c) 98% span

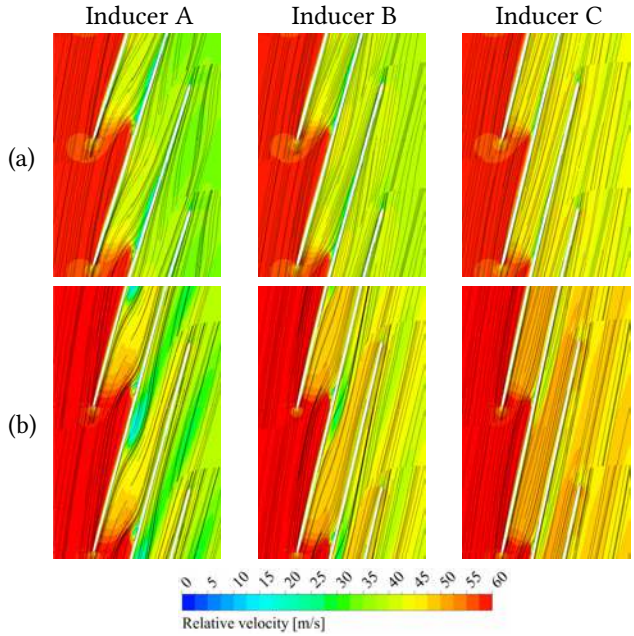

Figure 9. Relative velocity contours at: (a) 20% span and (b) 50% span

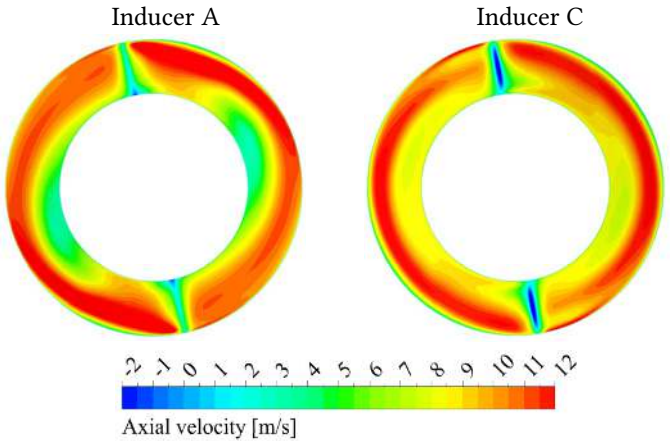

Figure 10. Axial velocity contours at 1% of the inducer axial length downstream of the trailing edge for inducer A and C

the suction side to the pressure side in order to align again with the blade pressure side. Both flow deflections are clearly visible in Figure 9(a) on the basis of the relative velocity distribution at 20% span. The bigger the flow separation area, the stronger is the deflection that the flow undergoes. The second flow deflection towards the circumferential direction in the hub region is directly related to a decrease of axial velocity, an increase of relative flow angle and tangential velocity (absolute), which can be observed in Figure 7.

The tangential velocity shows a slow increase towards the tip with a gradual distribution in the tip region for all three geometries. Generally, the tangential velocity is much higher than the design value and the discrepancy between design value and numerical results increases when the blade angle is reduced. Lakshminarayana [10] justifies the high tangential velocity values with real fluid effects combined with radial flows that exist inside the blade passage.

Despite the different trailing edge shape, the inducers show very little differences in the radial distribution of the velocity components and the velocity profiles are just shifted towards lower or greater values.

5. CONCLUSION

In the frame of the research project KonRAT at TUM a design methodology for turbopump components has been developed. In this paper the design process for the pump and especially for the inducer is described in detail. A numerical study on the influence of the incidence angle on the internal flow and on the performance was conducted on three flat-plate inducers with cylindrical hub and tip operating in liquid oxygen. In the numerical model, cavitation has been taken into account on the base of the Rayleigh-Plesset equation. The variation of incidence angle has been realized with two different approaches: The first two inducers were designed by keeping a fixed value of the incidence angle to blade angle ratio ν_B over the entire radius, whereas for the third inducer incidence angles at hub and tip have been assumed. Results

show that an inducer designed with the recommended value of 0.425 for ν_B considerably exceeds the requirement of 10% total head rise capability. The bigger the incidence angle, the larger is the discrepancy between design value and numerical results in terms of total pressure at outlet and velocitiy distribution at exit. Downstream of the trailing edge, the flow shows a tendency to separate near the hub. This is due to flow deflections in the blade passage caused by cavitation on the suction side on the first 1/3 of blade chord length. With increasing incidence angle, the amount of cavitation rises, the flow deflections become stronger causing considerable decrease of axial velocity at outlet and flow separation on the blade pressure side. Big discrepancies between effective velocity profiles and design values at inducer exit, on which the impeller is designed, also increase the number of iteration loops in the design process.

The objective of this paper is to better link the study of fluid mechanics of the internal flow with the cavitation behavior of an inducer. The first step in this direction is accomplished by reducing the inducer to its simplest form. Although the study is conducted on simple flat-plate inducer geometries, tendencies regarding the occurence of blade cavitation on the suction side as well as the flow behavior directly at the leading edge can be applied to more complex geometries such as cambered inducers which are more representative of the current technological standards. Surely, in order to confirm this supposition, the results obtained in this study and those obtained on similar geometries with cambered blading should be compared. It will be a further step to extend the design methodology by introducing the possibility to generate cambered inducer blades. The intention of the authors in starting from a very simple geometry and gradually introducing complexity is to be able to recognize the influence of single geometrical parameters in the complex flow behavior of state-of-the-art inducers so that targeted modifications of the geometry can be undertaken.

Further studies will cover the comparison between radial and swept back leading edges as well as the comparison between inducers with constant and variable hub contours. Furthermore, numerical simulations will be conducted by operating the inducers also in hot water in order to validate the numerical models with experimental data coming from the test facility at TUM [26].

ACKNOWLEDGMENTS

This project is supported by Ludwig Bölkow Campus, funded by the Bavarian government. The good cooperation with the consortium partners is appreciated.

NOMENCLATURE

C	Blade chord length
D_s	Specific diameter
H	Head rise
i	Incidence angle
L_{ax}	Blade axial length
N	Rotational speed
N_s	Specific speed
N_{ss}	Specific suction speed
NPSH	Net positive suction head
Q	Volume rate
S	Blade spacing
β	Relative flow angle
γ	Blade angle
δ	Deviation angle
η	Efficency
θ	Rolling up angle
ν_B	Incidence to blade angle ratio
$\phi = \frac{c_m}{u}$	Flow coefficent
$\psi = \frac{\Delta p}{\rho u^2}$	Head coefficient

Subscripts

0,1	inducer inlet, inducer outlet
h	hub
hyd	hydraulic
P	pump
t	tip

Abbreviations

LE	leading edge
LH2	liquid hydrogen
LOX	liquid oxygen
TE	trailing edge
TUM	Technical University of Munich

REFERENCES

[1] W. R. Bissel H. W. Douglass, A. J. Sobin. Turbopump systems for liquid rocket engines. *Series on NASA Space Vehicle Design Criteria*, NASA SP-8107, 1974.

[2] R. B. Keller Jr J. K. Jakobsen. Liquid rocket engine turbopump inducers. *Series on NASA Space Vehicle Design Criteria*, NASA SP-8052, 1971.

[3] A. J. Acosta. Flow in inducer pumps, an apercu. *Proceedings 4th International Symposium on Transport Phenomena and Dynamics of Rotating Machinery*, 1992.

[4] A. J Acosta, Y. Tsujimoto, Y. Yoshida, S. Azuma, and P. Cooper. Effects of leading edge sweep on the cavitating characteristics of inducer pumps. *International Journal of Rotating Machinery*, 7(6):397–404, 2001.

[5] F. Bakir, S. Kouidri, R. Noguera, and R. Rey. Experimental analysis of an axial inducer influence of the shape of the blade leading edge on the performances in cavitating regime. *Journal of fluids Engineering*, 125(2):293–301, 2003.

[6] A. Cervone, G. Pace, L. Torre, A. Pasini, S. Bartolini, L. Agnesi, and L. D'Agostino. Effects of the leading edge shape on the performance of an axial three bladed inducer. *14th International Symposium on Transport Phenomena and Dynamics of Rotating Machinery (ISROMAC-14)*, Honolulu, HI, 2012.

[7] O. Coutier-Delgosha, G. Caignaert, G. Bois, and J.-B. Leroux. Influence of the blade number on inducer cavitating behavior. *Journal of Fluids Engineering*, 134.8, 2012.

[8] S. Hong, J. Kim, C. Choi, and J. Kim. Effect of tip clearance on the cavitation performance of a turbopump inducer. *Journal of Propulsion and Power*, 22.1:174–179, 2006.

[9] S. Kim, C. Choi, J. Kim, J. Park, and J. Baek. Tip clearance effects on cavitation evolution and head breakdown in turbopump inducer. *Journal of Propulsion and Power*, 29.6, 2013.

[10] B. Lakshminarayana. Analytical and experimental study of flow phenomena in noncavitating rocket pump inducers. *NASA Contractor Report 3471*, October 1981.

[11] L. Veggi, J. D. Pauw, B. Wagner, T. Godwin, and O. J. Haidn. Numerical and experimental activities on liquid oxygen turbopumps. *5th Conference on Space Propulsion*, 2016.

[12] C. Maeding, L. Souverein, D. Hummel, S. Koenigbauer, A. Wagner, and J. Alting. A preliminary design study for an expander lox turbopump. *6th European Conference for Aeronautics and Space Sciences (EUCASS)*, Krakow, Poland, 2015.

[13] L. Souverein, C. Maeding, T. Aichner, B. Ivancic, A. Wagner, and M. Frey. Design and tool anchoring for a 120kn expander cycle rocket engine lox turbopump. *6th European Conference for Aeronautics and Space Sciences (EUCASS)*, Krakow, Poland, 2015.

[14] C. Bramanti. Experimental study of cavitation and flow instabilities in space rockets turbopumps and hydrofoil. *Doctoral dissertation*, University of Pisa, Italy, 2006.

[15] J. F. Gülich. Centrifugal pumps. *Berlin: Springer*, 2013.

[16] D. K. Huzel, D. H. Huang, and H. Arbit. Modern engineering for design of liquid-propellant rocket engines. *American Institute of Aeronautics and Astronautics*, Vol. 147, 1992.

[17] B. Lakshminarayana. Fluid dynamics of inducers- a review. *ASME, Transactions, Journal of Fluids Engineering*, 104:411–427, 1982.

[18] G. P. Sutton and O. Biblarz. Rocket propulsion elements. *John Wiley & Sons*, 2010.

[19] E. Logan Jr. Handbook of turbomachinery. *CRC Press*, 2003.

[20] P. R. Meng and R. D. Moore. Effect of blade leading edge thickness on cavitation performance of 80.6 deg helical inducer in hydrogen. *National Aeronautics and Space Administration*, NASA TN D-5855, 1970.

[21] K. Ashihara and A. Goto. Effects of blade loading on pump inducer performance and flow fields. *ASME 2002 Fluids Engineering Division Summer Meeting*, Montreal, Quebec, Canada, July 14-18, 2002.

[22] D. Kang, K. Yonezawa, H. Horiguchi, Y. Kawata, and Y. Tsujimoto. Cause of cavitation instabilities in three-dimensional inducer. *Proceedings of the 7th International Symposium on Cavitation*, Ann Arbor, Michigan, USA, August 17-22, 2009.

[23] F. Joussellin, Y. Courtot, O. Coutier-Delgosha, and J. L. Reboud. Cavitating inducer instabilities : experimental analysis and 2d numerical simulation of unsteady flow in blade cascade. *4th International Symposium on Cavitation*, Pasadena, 2001.

[24] F. Bakir, R. Rey, A. G. Gerber, T. Belamri, and B. Hutchinson. Numerical and experimental investigations of the cavitating behavior of an inducer. *International Journal of Rotating Machinery*, 10:15–25, 2004.

[25] F. Bakir, R. Rey, A. G. Gerber, T. Belamri, and B. Hutchinson. Numerical analysis of cavitating flows in rocket turbopump elements. *37th AIAA/ASME/SAE/ASEE Joint Propulsion Conference*, Salt Lake City, UT:AIAA 2001–3400, 2004.

[26] J. D. Pauw, L. Veggi, B. Wagner, J. Mondal, M. Klotz, and O. J. Haidn. Design procedure of a turbopump test bench. *17th International Symposium on Transport Phenomena and Dynamics of Rotating Machinery (ISROMAC-17)*, Maui, HI, 2017. (in review).